CrystEngComm

ROYAL SOCIETY OF CHEMISTRY

PAPER

View Article Online
View Journal | View Issue

Cite this: *CrystEngComm*, 2025, **27**, 7205

Heavily doped N-polar GaN with a mirror-like surface achieved *via* Ge doping

Yonghao Liu,[ab] Yuanhao Huang,[ab] Yang Jiang, *[ab] Hong Chen,[abc] Haiqiang Jia,[abc] Wenxin Wang,[ab] Chunhua Du[ab] and Zhen Deng[ab]

Received 5th June 2025,
Accepted 7th October 2025

DOI: 10.1039/d5ce00579e

rsc.li/crystengcomm

We used metal organic chemical vapor deposition (MOCVD) to grow germane (GeH_4) doped N-polar GaN on sapphire substrates with misorientations of 2° and 3° off *A*-plane (2A and 3A). At a GeH_4 doping flow rate of 156 nmol min^{-1}, a carrier concentration of 1.46×10^{20} cm^{-3} was achieved, and the surface morphology and crystal quality show almost no deterioration compared with undoped N-polar GaN (RMS = 0.821 nm and electron mobility μ = 89 cm^2 V^{-1} s^{-1}). As the GeH_4 flow rate increases, the doping concentration increases while the mobility decreases, and the surface morphology and crystal quality are less affected. However, if an excessively high doping flow rate is applied, the crystal quality will deteriorate, and pits will appear on the surface. The results of Raman spectroscopy show that as the doping flow rate increases, the compressive stress first increases and then decreases. We compared the GeH_4 doping of N-polar, Ga-polar, and non-polar GaN. At the same n++ doping level, only the N-polar GaN can maintain excellent crystal quality and surface undulation, which has important application potential for devices requiring heavily doped layers in the future.

Introduction

In recent years, the growth of heavily doped n-type GaN has attracted much interest of research institutions and universities around the world. Heavy n-doping has a wide range of applications in the fields of power electronic devices and optoelectronic devices. For example, it is used in distributed Bragg reflectors (DBRs),[1] polarization screening applications,[2] transparent current spreading layers for blue tunnel junction light emitting diodes,[3] and plasmonic detectors.[4] Under all these application conditions, there is a desire to obtain n-type materials with higher doping concentrations. As the most common n-type dopant, silicon has a concentration that is difficult to exceed 10^{19} cm^{-3}, and in the case of high doping, it will lead to many problems such as deterioration of the surface morphology, degradation of crystal quality, and the introduction of stress.[5] However, using germanium (Ge) as a dopant can avoid the above problems. It can achieve a doping concentration greater than 10^{20} cm^{-3}, and there will be no issues such as the introduction of stress or deterioration of the surface morphology.[6] Currently, research on the doping of Ge in GaN grown by MOCVD is mainly focused on Ga-polar GaN. The research group led by Dario Schiavon has thoroughly investigated the influence of the growth temperature and growth rate on the incorporation of Ge during the growth of Ga-polar GaN.[7] However, the obtained samples have a rough surface with macrosteps of 8 nm and 15 nm. The variation of surface undulation induced by doping has also been extensively studied in the growth of InN or Mg-doping processes.[18,19] Matthias Wieneke's research group has also achieved a doping concentration exceeding 10^{20} cm^{-3} on the *A*-plane GaN.[8] However, there were relatively few studies on the Ge doping of N-polar GaN. This paper explores Ge doping in N-polar GaN and obtains a heavily doped n-type thin film with a doping concentration reaching 10^{20} cm^{-3}. Compared with Ga-polar and non-polar GaN, its surface morphology, crystal quality, and stress conditions are less affected.

Experimental

All the N-polar GaN samples were grown using an AIXTRON G3 2400HT MOCVD system. Sapphire substrates are well-established industrial products in the market. The substrates include 2A (2° misorientation of the *A* plane {11_20}), and 3A sapphire substrates, with a diameter of two inches and a thickness of 430 μm, which is used to obtain high-quality N-polar gallium nitride thin films. The reaction precursors are trimethylgallium (TMGa) as the Ga source, ammonia (NH_3) as the N source, hydrogen (H_2) and nitrogen (N_2) as the carrier gases, and Ge supplied from a mixture of 5%

[a] *Key Laboratory for Renewable Energy, Beijing Key Laboratory for New Energy Materials and Devices, Beijing National Laboratory for Condensed Matter Physics, Institute of Physics, Chinese Academy of Sciences, Beijing 100190, China. E-mail: jiangyang@iphy.ac.cn*
[b] *University of Chinese Academy of Sciences, Beijing 100049, China*
[c] *Songshan Lake Materials Laboratory, Dongguan 523808, China*

Table 1 Summary of the growth conditions and characterization results of the samples, where only the misorientation angle and the GeH_4 flow were varied

Sample	GeH_4 (nmol min^{-1})	μ (cm^2 V^{-1} s^{-1})	n (10^{17} cm^{-3})	Doping efficiency (n/GeH_4)	FWHM of (002)	RMS (nm)	Residual stress (GPa)	FWHM of Raman shift (cm^{-1})
A1	0	178	34		61	0.882	0.26	3.28
A2	80	124	258	3.23	64	0.883	0.38	2.97
A3	156	89	1459	9.35	69	0.821	0.36	3.20
A4	405	96	2090	5.16	95	3.13	0.28	2.97
B1	0	174	35		353	1.40	0.16	2.73
B2	80	162	229	2.86	222	0.982	0.29	2.81
B3	156	92	1501	9.62	225	1.33	0.27	2.98
B4	405	99	2040	5.04	392	2.73	0.21	2.89

GeH_4 and 95% H_2 of six-nines purity as the Ge source. First, a 1 μm-thick undoped N-polar GaN layer was grown. After that, we introduced GeH_4 to grow n++ GaN with 0.5 μm. During the whole process, the flow rate of TMGa was 95 μmol min^{-1}, the flow rate of NH_3 was 44.64 mmol min^{-1}, and the growth temperature was 1190 °C. The Ge-doped GaN layer was grown with continuous GeH_4 flow. The total carrier gas flow was 18 000 sccm and the susceptor rotation was 10 rpm. The growth rate was 1 μm h^{-1}. Detailed growth conditions have been presented in our previous work.[9] For the experimental samples, we used an optical microscope and an atomic force microscope (AFM) to characterize the surface morphology, X-ray diffraction (XRD) to characterize the crystal quality, 300 K van-der-Pauw Hall-effect measurements to obtain the mobility and carrier concentration, and Raman spectroscopy to characterize the stress state of the materials.

Results and discussion

The growth conditions of the samples and the test results are shown in Table 1. Samples A1–A4 were grown on 2A substrates, and samples B1–B4 with 3A substrates.

Here, we adopt the n-type carrier concentration divided by the flow rate of GeH_4 introduced as doping efficiency. The larger this value, the more carrier concentration increases per unit of the introduced GeH_4, indicating a higher incorporation efficiency. From the doping efficiency results of samples A2–A4 and B2–B4 in Table 1, it can be seen that as the flow rate of GeH_4 increases, the doping efficiency of Ge first increases and then decreases. To analyze this phenomenon, we further increased the flow rate of GeH_4 and observed it with an optical microscope, using a 10× eyepiece and a 50× objective lens. As a result, pits appeared on the surface, and as the flow rate of GeH_4 further increased, these pits also became larger. As shown in Fig. 1, Fig. 1(a) and (b) were the surface of the samples when the GeH_4 flow rates were 892 nmol min^{-1} and 1339 nmol min^{-1} respectively. It can be seen that when the flow rate of GeH_4 is too high, the surface morphology deteriorates sharply, which is not conducive to the fabrication of devices. In the GeH_4 doping experiment of Ga-polar GaN, this kind of V-pit (hexagonal inverse-pyramidal pits) also appeared.[7] This surface morphology has been carefully studied before during the low-temperature growth (650–800 °C) of InGaN. V-pits were formed on top of screw (or mixed) dislocations.[10] The FWHM of the (002) plane in XRD measurements can well reflect the screw dislocation density of the sample *via* the formula: $D = FWHM^2/4.35b^2$, where D and b are the screw dislocation density and Burgers vector of screw dislocation, respectively. The phase separation of In is likely to occur here. Moreover, during the growth of InGaN *via* MOCVD, the temperature needs to be controlled at approximately 700 °C to suppress

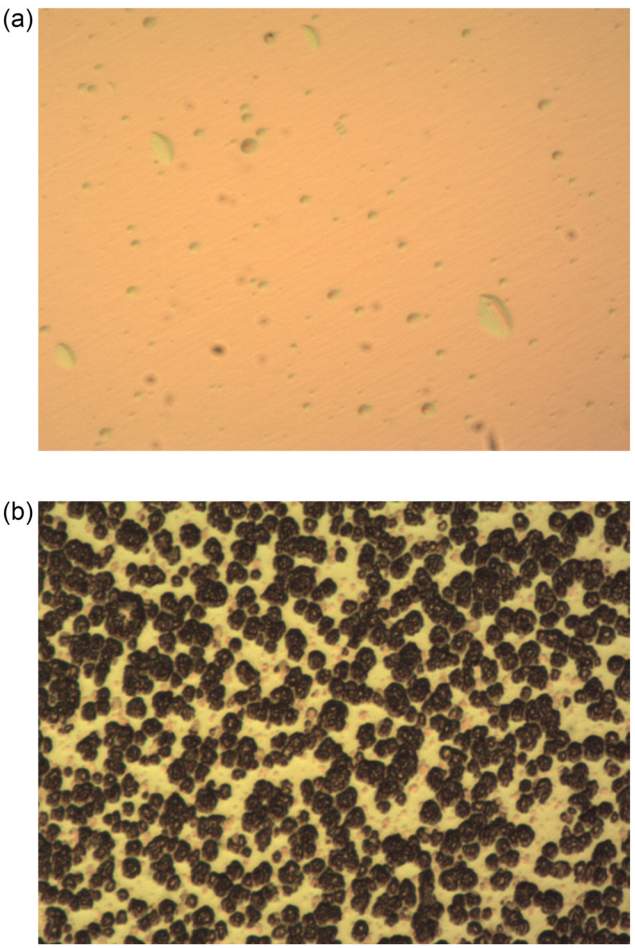

Fig. 1 Optical microscope image of the samples when the GeH_4 flow rates were 892 nmol min^{-1} (a) and 1339 nmol min^{-1} (b).

In volatilization. This relatively low temperature results in low surface mobility of In atoms, which are unable to eliminate stress concentration at dislocations through diffusion—ultimately leading to the formation of V-pits. However, when Ge was doped during the growth of GaN, these V-shaped pits may also be generated even at a temperature as high as 1075 °C.[11] The physical mechanism proposed to explain their formation involves the segregation of liquid germanium droplets on top of screw dislocations. The screw-type dislocation creates a step when terminating at

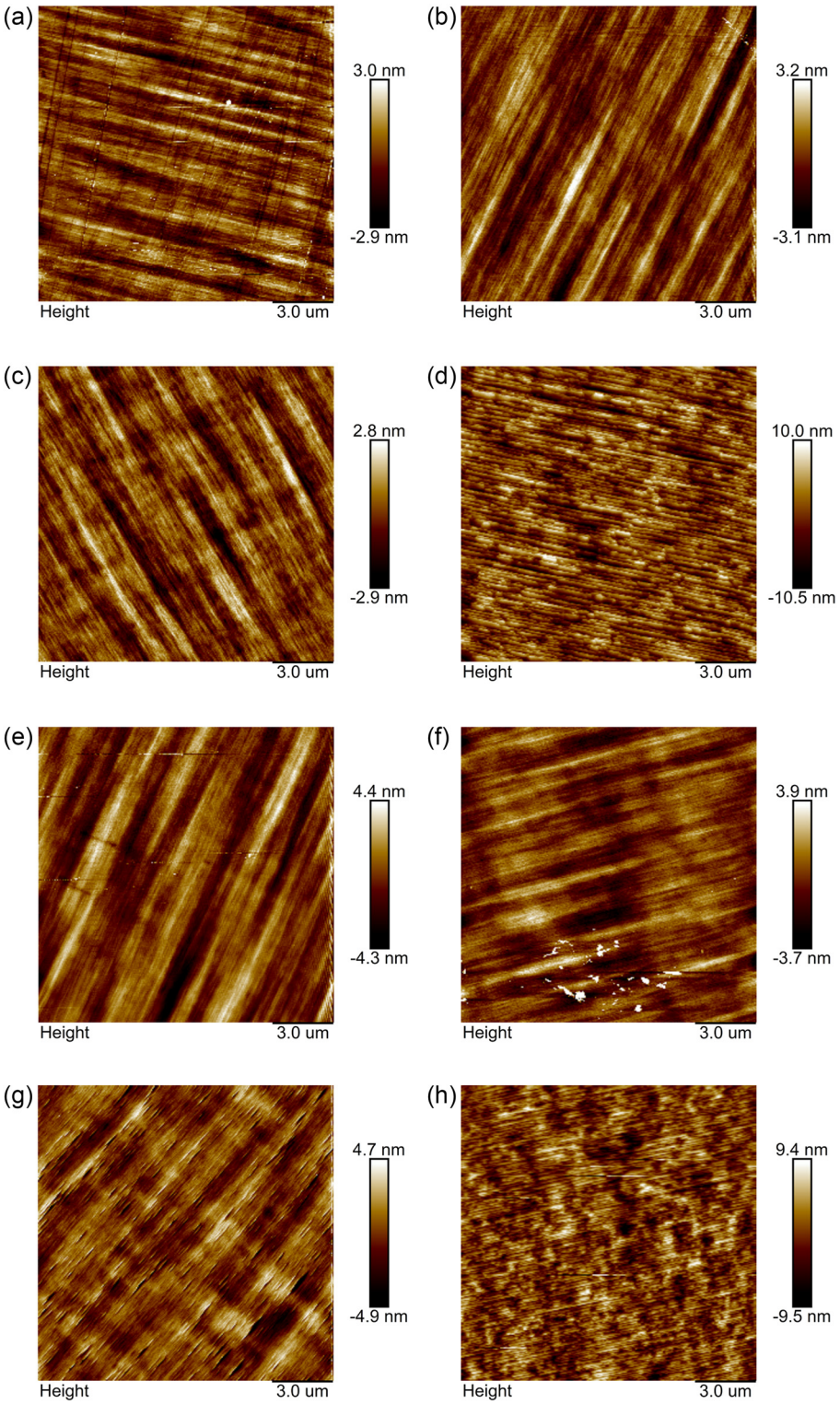

Fig. 2 The results of AFM. The scanning range is 15 μm × 15 μm. (a)–(d) represent A1–A4, respectively, while (e)–(h) represent B1–B4, respectively.

the GaN surface. This step facilitates the adsorption of impurities. When the Ge concentration exceeds the bulk solubility limit of Ge in GaN, the excess Ge atoms may nucleate at the dislocation and grow into clusters. Droplets appeared in the center of many pits in heavily doped samples. V-pits are then formed as a consequence of the disturbance provoked by the droplets themselves.[12,13] At the beginning, as the flow rate of GeH_4 increases, the doping efficiency gradually increases. Because the diffusion rate accelerates, which is more conducive to Ge atoms occupying the positions of Ga atoms to form donors. When the flow rate of GeH_4 further increases, the above-mentioned phenomenon of Ge precipitation at screw dislocations occurs inside the crystal and on the surface. This hinders the further diffusion of Ge atoms, leading to a decrease in doping efficiency. There is another possibility that the situation of Ge substituting for N atoms occurs, which we will analyze in the part of Raman test.

Next, we analyze the AFM test results of the samples. As shown in Fig. 2, when the GeH_4 flow rate is lower than 156 nmol min^{-1}, on the premise that the doping concentration can reach 10^{20} cm^{-3}, it hardly affects the surface morphology and the roughness. However, under the growth conditions of Ga-polarity and non-polarity, when the doping concentration reaches 10^{20} cm^{-3}, it will lead to obvious deterioration of the surface observed under an optical microscope and the appearance of V-shaped pits.[7,8,11] This may be caused by the quasi-two-dimensional growth and step growth mode on misorientation substrates during N-polar GaN growth. Dario Schiavon's research group also found that when growing Ga-polar Ge-doped GaN, the lack of V-pits in samples grown at low temperature was always connected to the emergence of step bunching.[7] However, when the GeH_4 flow rate is higher, as shown in Fig. 2(d) and (h), the surface undulation increases rapidly, which is not conducive to the growth of materials and fabrication of future devices. This may be attributed to the segregation of liquid germanium droplets on top of screw dislocations mentioned above. Therefore, when materials or devices require a relatively flat surface morphology, it is necessary to consider that there is a maximum limit for the introduction of the GeH_4 flow rate.

As can be seen from Fig. 3, for the 2A and 3A substrates, as the GeH_4 flow rate increases, the mobility gradually decreases while the doping concentration keeps increasing. This may be caused by the fact that the doping of Ge atoms disrupts the regular lattice periodicity of the GaN crystal, generating more disturbances and leading to a decrease in the electron mobility. The GeH_4 doping flow rate of samples A3 and B3 is 156 nmol min^{-1}, and at this time, the doping concentration can already reach 10^{20} cm^{-3}. If the doping flow rate further increases, the carrier concentration will not increase significantly. In contrast, it may lead to the surface V-pits problem mentioned above. There are two possible reasons for the decrease in mobility. On the one hand, higher doping may lead to the destruction of the lattice periodicity, generating more disturbances and intensifying the lattice

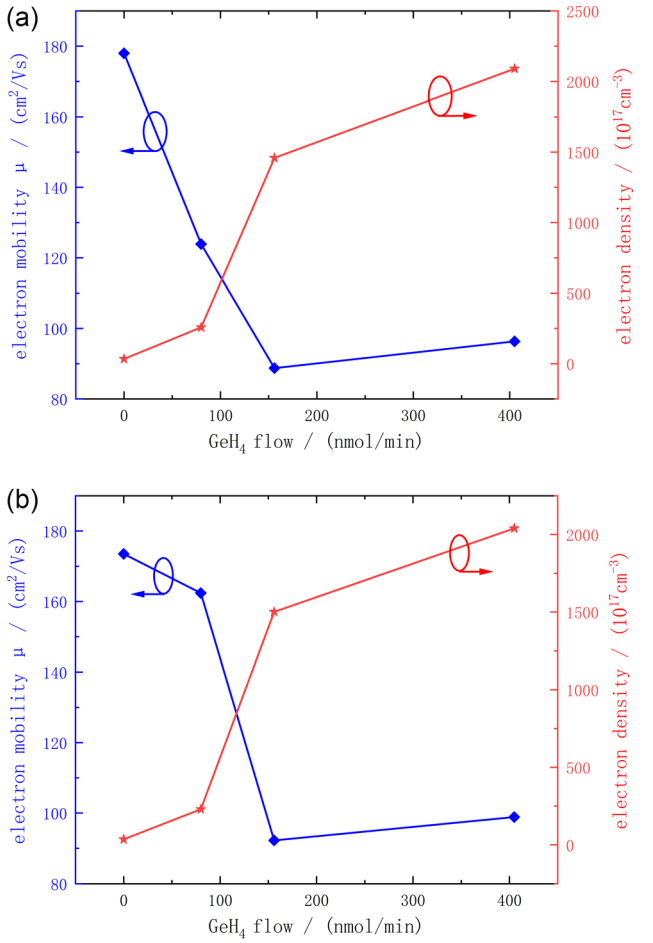

Fig. 3 The relationship between the electron mobility, doping density and GeH_4 flow rate of A1–A4 (a) and B1–B4 (b).

vibration scattering. On the other hand, a higher carrier concentration may lead to an enhancement of the Coulomb interaction between carriers. As the results between A3, A4 and B3, B4 show, the carrier concentration increases only slightly, the mobility also changes gently.

The XRD test results of the samples are shown in Fig. 4. For samples A1–A4, when the GeH_4 flow rate is lower than 156 nmol min^{-1}, as flow rate increases, the crystal quality of the samples basically shows no tendency of deterioration. This indicates that GeH_4 does not introduce extra screw dislocations. When the flow rate further increases, the full width at half maximum (FWHM) data increases significantly, indicating more screw dislocations. This may be attributed to the appearance of pits as the GeH_4 flow rate increases, or greater changes in the lattice periodic structure caused by higher doping. For samples B1–B4, as the GeH_4 flow rate increases, the change in the FWHM value shows a trend of decreasing first and then increasing. We speculate that during the process of GeH_4 doping, Ge atoms will preferentially occupy the sites generated by screw dislocations. For the 2A substrate, the original screw dislocation level is relatively low, so the introduction of GeH_4 has almost no impact on the screw

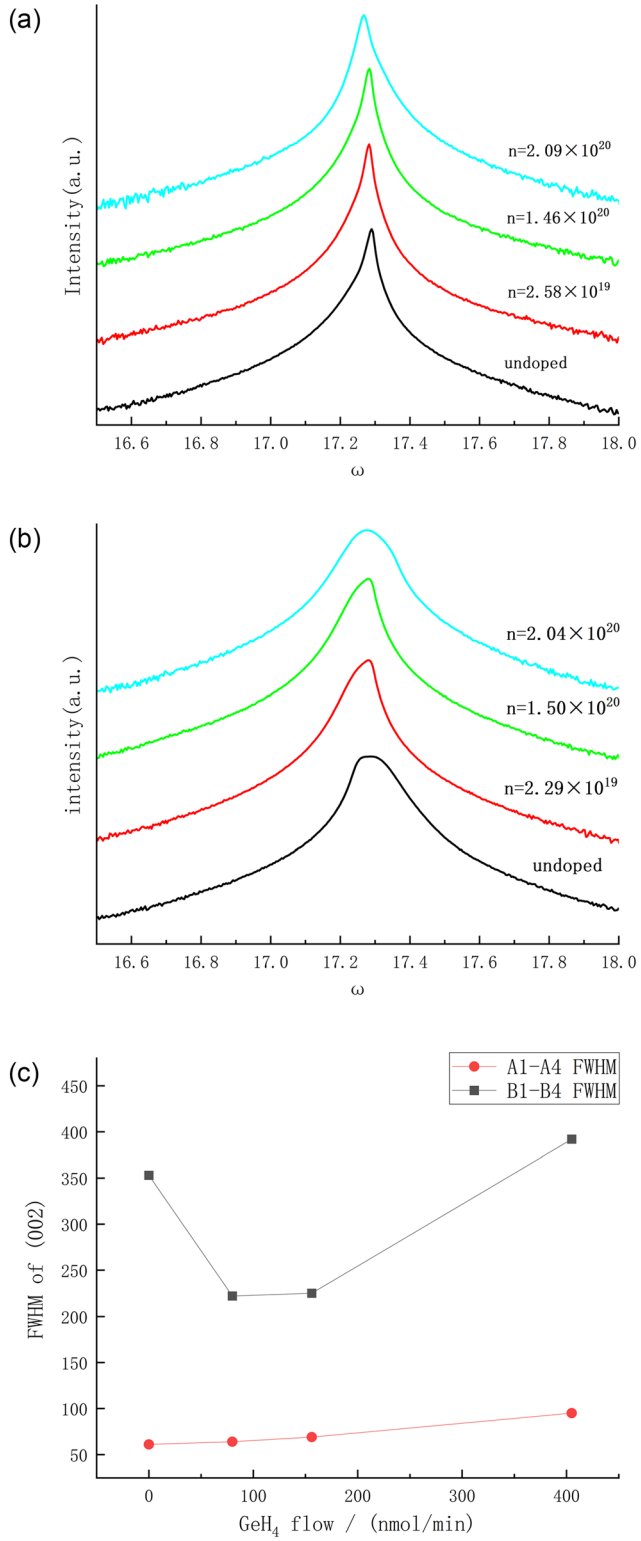

Fig. 4 The XRD test and FWHM results of (002) for A1–A4 (a) and B1–B4 (b) and the relationship between the FWHM of all the samples and GeH_4 flow rate (c).

dislocations. However, for the 3A substrate, the screw dislocation level in the undoped state is relatively high. At this time, Ge atoms occupy the screw dislocation sites, which inhibit the generation and extension of screw dislocations to a certain extent.

When it is necessary to evaluate the strain condition, crystal quality and carrier concentration of semiconductor materials, Raman spectroscopy is a relatively common and accurate method, and it also has the advantage of spatial resolution limited only by diffraction. For the non-polar modes in the wurtzite crystals (such as GaN), for example, the E2 (high) mode, it is an ideal tool for determining the stress; while the polar modes, such as the longitudinal optical mode and the transverse optical mode (LO mode and TO mode), due to their coupling with plasmons, can be directly used to determine the carrier concentration and carrier mobility. Fig. 5(a) and (b) are the Raman spectroscopy results of samples A1–A4 and B1–B4, respectively. In the relaxed bulk GaN, the E2 (high) mode peak position is 568 cm^{-1}.[14] As can be seen from Fig. 5(c), the E2 (high) mode peak positions of all the samples have undergone a blue shift to varying degrees, which indicates that the grown crystals are under compressive stress. In order to further explore the residual stress situation of the thin film, the stress value σ is calculated through the following formula:[15]

$$\Delta\omega = k\sigma$$

where $\Delta\omega$ is the peak shift value of Raman spectra, and k is the stress factor. The residual stress test results of all the samples are listed in Table 1. As can be seen from Table 1 and Fig. 5(c), the larger the misorientation angle, the smaller the stress. This is because the misoriented substrate is designed to adapt to the quasi-two-dimensional growth mode of N-polar GaN.[16] A larger misorientation angle means that more low-energy sites are actively introduced to facilitate the migration of Ga atoms during growth. The GaN lattice at these sites can better match the substrate lattice, which can release stress to a certain extent.

As GeH_4 is introduced, the compressive stress of all samples shows the characteristic of first increasing and then being relieved. The atomic radius of Ga, Ge, and N is 130 pm, 122 pm, and 74 pm, respectively. In the initial doping stage, Ge basically replaces Ga to become a donor atom. The smaller atomic radius of Ge causes compressive stress inside the lattice, and a blue shift occurs. However, the subsequent release process of compressive stress is still confusing. The research group led by Xuelin Yang, when studying the C doping of GaN grown on a Si substrate, found that with the increase of the C concentration, the Raman scattering results of the GaN thin film first show a red shift and then a blue shift.[17] It is possible that C first occupies the N position, causing the lattice to generate tensile stress. As the C doping concentration gradually increases, C begins to occupy the Ga position, resulting in the lattice generating compressive stress. Here, it may also be caused by a similar reason, given that both Ge and C are group IV elements. With the increase of doping, some Ge begins to replace N, relieving the compressive stress state of

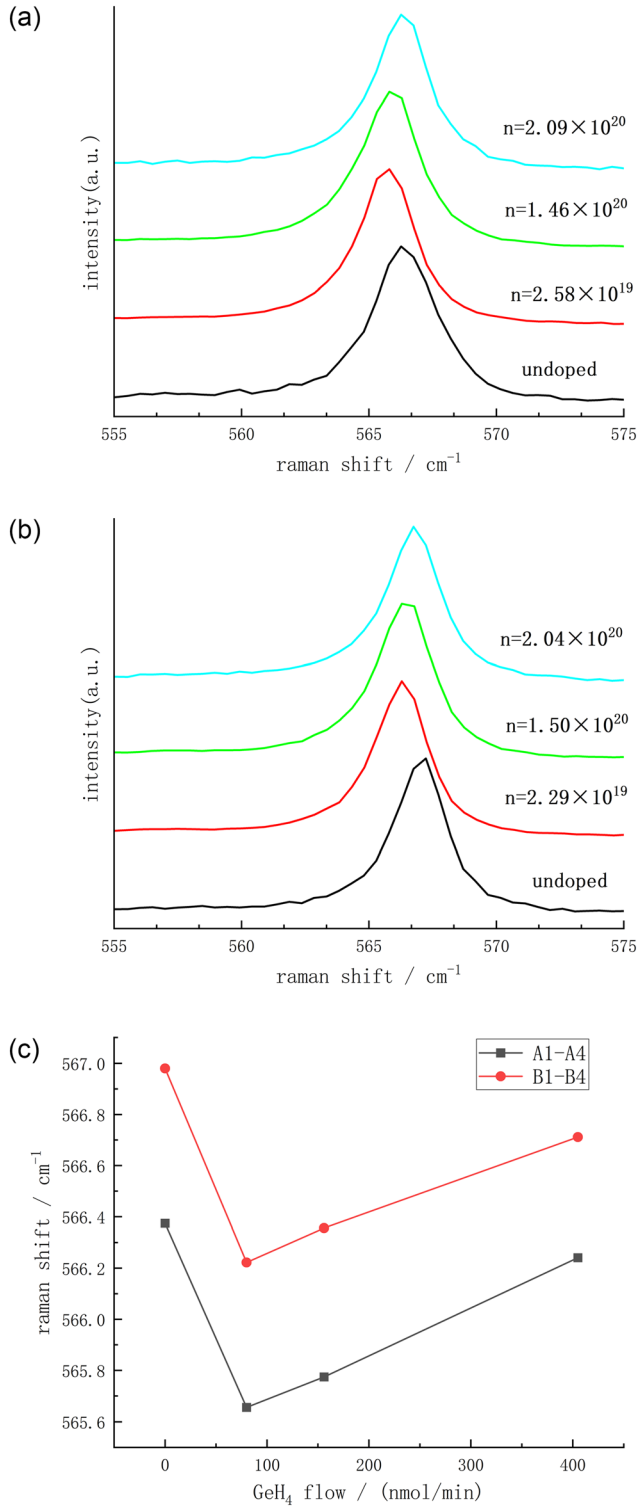

Fig. 5 Raman spectroscopy results of A1–A4 (a) and B1–B4 (b) and the Raman peaks of all the samples (c).

the entire lattice. However, this remains a tentative speculation of our group. As for the phenomenon of increased Raman peak wavelength induced by higher doping concentration, we acknowledge that further theoretical calculation analysis and experimental verification are necessary, and we plan to conduct this work in subsequent studies.

As can be seen from Table 1, with the change of the GeH_4 doping flow rate, the FWHM of the Raman peaks changes extremely small. For samples A1–A4 grown on the 2A substrate, the maximum change in FWHM is less than 0.35 cm^{-1}. For samples B1–B4 grown on the 3A substrate, the maximum change in the FWHM is less than 0.3 cm^{-1}, which is better than the cases of Ge doping and Si doping in Ga-polar GaN (the maximum changes in the FWHM are 0.4 cm^{-1} and 0.7 cm^{-1} respectively).[6] This indicates that for the growth of N-polar GaN, GeH_4 doping causes less damage to the lattice structure.

To further explore the doping uniformity of Ge, we performed SIMS test on sample B3 using the CAMECA 7f-auto system, as shown in Fig. 6. There was no significant change in the oxygen (O) concentration of the sample, which remained consistently around 2×10^{18} atoms per cm^3. However, the carbon (C) doping concentration showed a certain increase after doping, rising from approximately 1.5×10^{16} atoms per cm^3 to around 3×10^{16} atoms per cm^3. Regarding the Ge content, its concentration was consistently higher than 1×10^{20} atoms per cm^3 within 0.1 μm from the surface, and then gradually decreased to 1×10^{19} atoms per cm^3 in the depth range of 0.1 μm to 0.5 μm. The introduction of Ge requires a growth thickness of approximately 50 nm to achieve the target doping concentration.

The previous text has a detailed analysis of the material characterization of the grown Ge-doped N-polar GaN samples. We can see that when the GeH_4 flow rate is 156 nmol min^{-1} (*i.e.*, samples A3 and B3), not only a high doping concentration level can be obtained, but also the surface morphology and crystal quality of the samples are basically not affected. Here, we compare the results of this work with the results of Ga-polar and non-polar Ge doping. The comparison results are shown in Table 2.

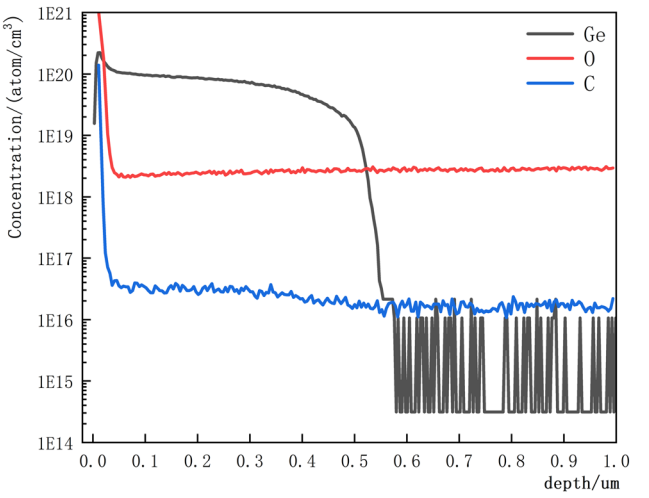

Fig. 6 SIMS measurement of Ge, C and O for sample B3.

Table 2 Research of Ge doping of different polar GaN

Research group	Sample	Ge precursor	Ge/Ga precursor (10^{-3})	n (10^{20} cm^{-3})
This work	N-polar(A3)	GeH_4	1.64	1.46
	N-polar(B3)	GeH_4	1.64	1.50
M. Wieneke[8]	Nonpolar	IBGe	105.2	1.34
	Nonpolar	IBGe	210.5	1.69
Dario	Ga-polar	GeH_4	95	0.44
Schiavon[7]	Ga-polar	GeH_4	720	1.80
S. Fritze[11]	Ga-polar	GeH_4	500	1.90
	Ga-polar	IBGe	500	1.50

As can be seen from Table 2, for the three different polarities of GaN, the carrier concentration of 10^{20} cm^{-3} can be achieved through different Ge sources. However, the GeH_4 flow rate required for Ge doping of N-polar GaN is much lower than that for non-polar and Ga-polar GaN, indicating that the incorporation efficiency of N-polar GaN is the highest. Moreover, when the research groups led by Dario Schiavon[7] and S. Fritze[11] carried out the GeH_4 doping experiment, the flow rate of GeH_4 was already at the same order of magnitude as that of TMGa, which is relatively unfavorable for crystal growth. M. Wieneke's research group studied the doping of the non-polar *A*-plane GaN.[8] When the doping concentration reached 1.69×10^{20} cm^{-3}, the crystal surface had already shown obvious deterioration under the optical microscope. Dario Schiavon's research group conducted a series of studies on Ge doping with varying conditions.[7] At a doping concentration of 7.6×10^{19} cm^{-3}, undulations of 3 to 10 nm had already appeared on the surface as observed under an AFM microscope, and the mechano-chemical polishing (MCP) technique was required for flattening treatment. The research group led by S. Fritze showed an optical microscope image with the IBGe doping concentration reaching 6×10^{19} cm^{-3} in their paper, and surface undulations and sporadic black holes could already be seen.[11] In contrast, samples A3 and A4 in this work not only have a doping concentration exceeding 10^{20} cm^{-3}, but also maintain a crystal quality level and surface undulation size very close to those of undoped N-polar GaN. This is of great significance for the fabrication of devices that require heavily n-doped GaN in the future.

Conclusions

We have thoroughly investigated the influence of GeH_4 doping on N-polar GaN. As the flow rate of GeH_4 increases, the carrier concentration first increases and then gradually reaches saturation, while the mobility decreases and gradually levels off. There is a critical value for the flow rate of GeH_4. Before reaching this value, the N-polar GaN film can achieve a carrier concentration on the order of 10^{20} cm^{-3}, and the crystal quality and surface morphology are hardly affected. We analyzed the stress situation of the samples using Raman spectroscopy. As the doping concentration increases, the compressive stress of the samples first increases and then decreases, which may be caused by the substitution growth of Ge atoms. Finally, we conducted a detailed comparison of the experimental results of Ge doping for GaN with different polarities. We found that for N-polar GaN, a much lower flow rate of GeH_4 is required to achieve the same doping concentration level. Moreover, the XRD characterization of crystal quality and the AFM characterization of the surface show that there is almost no impact caused by doping.

Author contributions

Yonghao Liu: conceptualization, data curation, formal analysis, investigation, methodology, software, visualization, writing – original draft, writing – review & editing. Yuanhao Huang: data curation, conceptualization. Yang Jiang: investigation, project administration, funding acquisition, writing – review & editing. Hong Chen: supervision, validation, resources. Haiqiang Jia: supervision. Wenxin Wang: validation. Chunhua Du: conceptualization. Zhen Deng: conceptualization.

Conflicts of interest

There are no conflicts to declare.

Data availability

All the data supporting this article have been included within the article and are available upon request.

Acknowledgements

This work was supported by the National Natural Science Foundation of China (Grant no. 62350002).

Notes and references

1 C. Seneza, C. Berger, P. Sana, H. Witte, J. Bläsing, A. Dempewolf, A. Dadgar, J. Christen and A. Strittmatter, *Jpn. J. Appl. Phys.*, 2022, **61**(1), DOI: 10.35848/1347-4065/ac3d43.
2 N. G. Younga, R. M. Farrell, M. Iza, S. Nakamura, S. P. DenBaars, C. Weisbuch and J. S. Speck, *J. Cryst. Growth*, 2016, **455**, 105–110, DOI: 10.1016/j.jcrysgro.2016.09.074.
3 C. Berger, S. Neugebauer, F. Hörich, A. Dadgar and A. Strittmatter, *J. Appl. Phys.*, 2022, **132**(23), 233103, DOI: 10.1063/5.0130757.
4 R. Kirste, M. P. Hoffmann, E. Sachet, M. Bobea, Z. Bryan, I. Bryan, C. Nenstiel, A. Hoffmann, J.-P. Maria, R. Collazo and Z. Sitar, *Appl. Phys. Lett.*, 2013, **103**(24), 709–713, DOI: 10.1063/1.4848555.
5 H. Ishikawa, K. Yamamoto, T. Egawa, T. Soga, T. Jimbo and M. Umeno, *J. Cryst. Growth*, 1998, **189–190**, 178–182, DOI: 10.1016/S0022-0248(98)00223-1.
6 C. Nenstiel, M. Bügler, G. Callsen, F. Nippert, T. Kure, S. Fritze, A. Dadgar, H. Witte, J. Bläsing, A. Krost and A. Hoffmann, *Phys. Status Solidi RRL*, 2015, **9**(12), 716–721, DOI: 10.1002/pssr.201510278.

7 D. Schiavon, E. Litwin-Staszewska, R. Jakieła, S. Grzanka and P. Perlin, *Materials*, 2021, **14**(2), 354, DOI: **10.3390/ma14020354**.
8 M. Wieneke, H. Witte, K. Lange, M. Feneberg, A. Dadgar, J. Blasing, R. Goldhahn and A. Krost, *Appl. Phys. Lett.*, 2013, **103**(1), 241109, DOI: **10.1063/1.4812666**.
9 Y. Liu, Y. Huang, Y. Jiang, H. Chen, H. Jia, W. Wang, C. Du and Z. Deng, *Vacuum*, 2025, **238**, 114294, DOI: **10.1016/j.vacuum.2025.114294**.
10 I.-H. Kim, H.-S. Park, Y.-J. Park and T. Kim, *Appl. Phys. Lett.*, 1998, **73**(12), 1634–1636, DOI: **10.1063/1.122229**.
11 S. Fritze, A. Dadgar, H. Witte, M. Bugler, A. Rohrbeck, J. Blasing, A. Hoffmann and A. Krost, *Appl. Phys. Lett.*, 2012, **100**(12), 011001, DOI: **10.1063/1.3695172**.
12 M. Iwinskaa, N. Takekawab, V. Yu. Ivanovc, M. Amilusika, P. Kruszewskia, R. Piotrzkowskia, E. Litwin-Staszewskaa, B. Lucznika, M. Fijalkowskia, T. Sochackia, H. Teisseyrea, H. Murakamib and M. Bockowski, *J. Cryst. Growth*, 2017, 102–107, DOI: **10.1016/j.jcrysgro.2017.10.016**.
13 Y. Zhang, J. Wang, X. Su, D. Cai, Y. Xu, M. Wang, X. Hu, S. Zheng, L. Xu and K. Xu, *Jpn. J. Appl. Phys.*, 2019, **58**(12), 120910, DOI: **10.7567/1347-4065/ab56f5**.
14 H. Harima, *J. Phys.: Condens. Matter*, 2002, **14**(38), R967, DOI: **10.1088/0953-8984/14/38/201**.
15 T. Kozawa, T. Kachi, H. Kano, H. Nagase, N. Koide and K. Manabe, *J. Appl. Phys.*, 1995, **77**(9), 4389–4392, DOI: **10.1063/1.359465**.
16 Q. Sun, Heteroepitaxy of nitrogen-polar, nonpolar, and semipolar gallium nitride by MOCVD[M], *PhD*, Yale University, 2009.
17 X. Yang, J. Shen, Z. Cai, Z. Chen and B. Shen, *Appl. Phys. Express*, 2022, **15**(10), 105501, DOI: **10.35848/1882-0786/ac8d49**.
18 Z. Benzarti, A. Khalfallah and Z. Bougrioua, *et al.*, *Mater. Chem. Phys.*, 2023, **307**, 128182, DOI: **10.1016/j.matchemphys.2023.128182**.
19 A. Z. Benzarti, *et al.*, *J. Alloys Compd.*, 2021, **885**, 160951, DOI: **10.1016/j.jallcom.2021.160951**.